metals

MDPI

Article

Corrosion Resistance and Ion Release of Dental Prosthesis of CoCr Obtained by CAD-CAM Milling, Casting and Laser Sintering

Roberto Padrós [1], Luís Giner-Tarrida [2], Mariano Herrero-Climent [3], Miquel Punset [4,5] and Francisco Javier Gil [2,6,*]

1 Barcelona Dental Institute, 08034-Barcelona, Spain; robertopadros@hotmail.com
2 Faculty of Dentistry, International University of Catalonia, Josep Trueta s/n, 08195 Barcelona, Spain; lginer@uic.es
3 Porto Dental Institute, 4150-518 Porto, Portugal; dr.herrero@herrerocliment.com
4 Biomaterials, Biomechanics and Tissue Engineering group (BBT), Department of Materials Science and Engineering, Universitat Politècnica de Catalunya (UPC), Av. Edurad Maristany 16, 08019 Barcelona, Spain; miquel.punset@upc.edu
5 UPC Innovation and Technology Center (CIT-UPC), Technical University of Catalonia (UPC), C. Jordi Girona 3-1, 08034 Barcelona, Spain
6 Bioengineering Institute of Technology, International University of Catalonia, Josep Trueta s/n, 08195 Barcelona, Spain
* Correspondence: xavier.gil@uic.cat

Received: 2 May 2020; Accepted: 16 June 2020; Published: 21 June 2020

Abstract: Corrosion resistance and ion release behavior have been evaluated for thirty dental restoration samples obtained by three different manufacturing systems: computer-aided design and manufacturing (CAD-CAM), traditional casting and laser sintering. The alloy used was the CoCr alloy (same batch) generally used in clinical dentistry. Corrosion resistance has been evaluated by electrochemical testing in an artificial saliva medium at 37 °C. Corrosion parameters such as critical current density (i_{cr}), corrosion potential (E_{corr}), and passive current density (i_p), have been determined. Cobalt and Chromium ions released from the different samples have also been analyzed in an artificial saliva medium at 37 °C by Inductively Coupled Plasma Mass Spectrometry (ICP-MS) at different immersion times. The casted samples showed higher corrosion rates and ion-release levels. The CAD-CAM milled samples presented lower ion-release levels and better corrosion resistance due to the total solubility of the chemical elements in only one phase with the same chemical composition. This homogeneity avoids the formation of electrochemical corrosion. Moreover, the absence of defects and residual stresses increases the corrosion resistance. Casted and laser sintered prostheses have shown the presence of Cr, W, and Nb rich-precipitates which are detrimental to the corrosion resistance. These precipitates produce a decrease in the Cr content on the surface. It is well known that the corrosion resistance increases with the Cr content by the formation of Chromium oxide on the surface that increases passivation. Consequently, the decrease in Cr induces an increase in corrosion and ion release.

Keywords: prosthesis; dental restorations; CAD-CAM; laser sintering; casting; corrosion; ion release; CoCr

1. Introduction

Corrosion of dental alloys is a major concern in dental restorations that can have a negative effect on the biology, function, and esthetic behavior of dental prosthesis. The process of corrosion releases

metal ions that may come into contact with the surrounding cells and tissues, even being distributed throughout the body flowing into the bloodstream, mainly moving through the intestine canal to the urinary excretory system. Corrosion and metal ion release can produce a decrease in the mechanical properties, cytotoxicity, adverse reactions to metal debris (ARMD) effects both at oral and systemic level, as well as the risk of developing sensitivity to metals [1–7].

The oral cavity is an aggressive medium due to the complex biological and electrolyte environment, which is affected by a wide range of factors including the presence of saliva, dental plaque, bacteria, gastric acid reflux, as well as by oxygen levels. In addition to the aforementioned biological factors, dental restorations are subjected, in the oral cavity, to extremely high mechanical loading due to mastication, as well as to permanent fluctuations in temperature and pH [5–7]. These aggressive conditions promote both corrosion and ion-release degradation mechanisms of metallic restoration materials used in dentistry. Consequently, corrosion products released from dental alloys can cause undesired side effects, such as local toxic, systemic toxic or allergic reactions in the immediate proximity of the dental restoration or in other areas in the human organism [8].

The CoCr base alloys' fabrication method using traditional methods based on casting is a difficult task. Several factors have hindered the fabrication of biomedical devices with CoCr-based alloys through conventional processes based on casting, plastic deformation, and machining. Among several aforementioned factors, high melting points, limited ductility, and high hardness values are probably the main drawbacks of using these alloys, given their limited workability [9].

Traditionally, dental metallic restorations were mainly fabricated by lost-wax conventional casting methods. These traditional methods include several procedures and/or steps with high handicraft (artisanal) components, which are based on classic conformation methods including milling and turning subtractive methods, plastic deformation, and casting. For the last few decades, substantial efforts have been made to develop new manufacturing technologies in order to overcome the drawbacks of conventional fabrication processes. Dental manufacturing has experienced a continuous evolution from traditional methods—such as casting to computer-aided design and manufacturing methods—which entailed an even higher degree of technical sophistication. Currently, in this respect, there is a wide range of different manufacturing technologies commercially available to produce CoCr dental prosthesis including both removable dental prostheses (RDPs) and fixed dental prostheses (FDPs), such as computer-aided design and manufacturing (CAD-CAM) milling [10,11], direct metal laser sintering (DMLS) [12–15], and Selective Laser melting (SLM) [16,17], among others.

The use of both pre-manufactured blocks and computer-aided automatized scanning and milling procedures can decrease the influence of human error in the manufacturing process to produce higher quality dental restorations. The combined use of CAD-CAM automated milling systems together with intraoral scanners, allows for prosthesis obtaining with finer details and excellent reproducibility [18–22]. Laser sintering is another latest generation modern technique characterized by a high production capacity together with excellent marginal accuracy, which makes it a very attractive alternative from an economic point of view. Despite the inherent constraints associated with the traditional casting process, casting modified techniques are actually used for the manufacture of dental restoration including slip casting, as well as injection and hot-pressing casting, which are selected depending on the restoration material used [3,18,19,22–32].

There are many studies focused on the marginal fit evaluation using different CAD-CAM systems, or other manufacturing processes, on dental metallic and ceramic restorations. However, only a few publications have focused specifically on both the corrosion and ion release behaviors of CoCr dental restoration prostheses produced by casting, CAD-CAM milling, or laser sintering [33]. Thus, it is crucial to increase knowledge on both advantages (strengths) and limitations (weaknesses) of each manufacturing process in order to ensure the optimal manufacturing process selection most suitable in any given clinical case.

The aim of this contribution focuses on the comparison between three different manufacturing methods in terms of corrosion and metal ion-release behaviors in artificial saliva at 37 °C, tested with the same batch of the CoCr alloy.

2. Materials and Methods

Thirty disk-shaped samples of 2 mm in diameter and 3 mm in height were manufactured by means of different manufacturing methods for dental prosthesis fabrication with the same batch of CoCr alloy. The chemical composition of the alloys is given in Table 1.

Table 1. Chemical composition of CoCr alloy.

Co	Cr	W	Si	C	Nb
56.53 ± 2.11	27.11 ± 1.31	9.64 ± 0.79	1.27 ± 0.80	<1%	<1.5%

Ten samples were made by a CAD-CAM system using a 5-axis milling cutter unit machine (Zfx-Sauer 10, Zimmer, Dachau, Germany), ten were manufactured employing traditional procedures, such as investment casting, using a lost-wax technique with a coating of phosphate and the other ten with a laser sintering method by means of a Ytterbium laser machine. The material used was powder from 0.01 to 0.1 mm in diameter. The samples were verified and calibrated in relation to the dimensions and volume of the structure.

They were polished metallographically following the recommendations defined in the ASTM E3-17 Standard [34]. Samples were first embedded in polymeric conductive resin followed by several sequential grinding steps with different silicium carbide (SiC) papers. Samples were finally polished using diamond suspension paste with an average particle grain size ranging from 5 to 0.1 µm (Buehler S4, Lake Bluff, IL, USA). All metallic disc-shaped samples were smoothed up to a surface roughness (Ra) under 20 nm. Upon completion of the polishing phase, samples were cleaned with a sequential immersion bath protocol using cyclohexane, isopropanol, ethanol, deionized water, acetone, and ethanol for 15 min for each cleaning bath together with sonication (all chemicals from Sigma Aldrich, St. Louis, MO, USA).

Testing sample groups were kept individually immersed in a constant volume of electrolyte for all the measurements. Artificial saliva was selected as an electrolyte in order to simulate the real oral physiological conditions, for which the composition is given in Table 2. The electrolyte was kept under constant conditions of temperature (37 °C) and pH (6.7) during the experiments, which was completely renewed for each experiment [35–38].

Table 2. Composition of artificial saliva used as an electrolyte for the corrosion test.

Chemical Product	Composition (g/dm^3)
K_2HPO_4	0.22
KCI	1.19
KSCN	0.29
Na_2HPO4	0.26
NaCl	0.69
$NaHCO_3$	1.49
Urea	1.49
Lactic acid	up to pH = 6.8

A group of five specimens (n = 5) were tested by means of electrochemical methods for each manufacturing process evaluated. The schematic electrical set-up diagram used to measure the

electrochemical parameters is shown in Figure 1. A glass corrosion cell type with a three-electrode array was used for electrochemical testing. Saturated calomel electrode (SCE) was used as a reference electrode (RE) (Vidra Foc, Barcelona, Spain). A Pt-electrode was axially inserted into the corrosion-cell as a counter-electrode or auxiliary electrode (AE) in order to ensure a homogeneous current distribution. The distance between the electrodes remained constant at 25 mm during all measurements. The open-circuit potential (OCP) of the working electrode (WE) samples was recorded after 250 min of immersion, guaranteeing potential stabilization, according to all relevant requirements detailed in the ASTM G5-14 Standard [39].

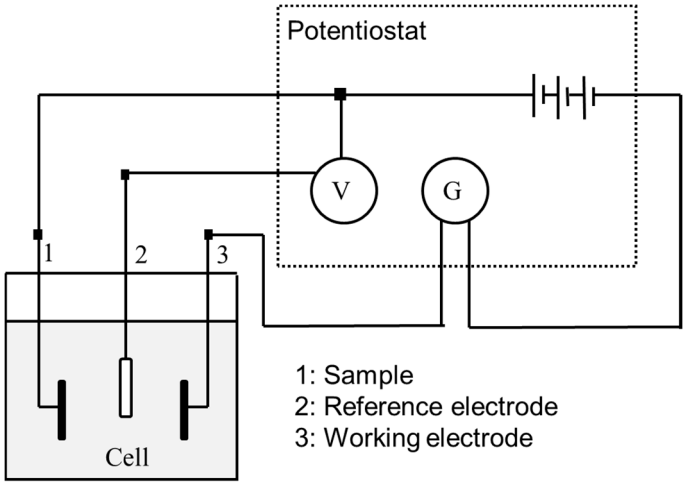

Figure 1. Three-electrode electrical circuit set-up diagram used in electrochemical tests.

The current versus time in the three electrode cell disposition used was controlled by a Hewlett Packard HP5 potentiostat (Palo Alto, CA, USA). Potential variation in an open short circuit was controlled by a Digital Multimeter and Scanner Resistance (Voltalab Radiometer VS89, Barcelona, Spain). The overall system was controlled using a PC-compatible computer. Corrosion tests and sample preparations were carried out following specifications proposed by ASTM G8 and ASTM G15 international Standards [34,39].

Samples were subjected to a two-step testing cycle. Firstly, starting with an immersion step in the de-aerated electrolyte during a 250 min period, during which the open circuit potential (OCP) of each working electrode was properly recorded. Subsequently, potentiodynamic polarization curves were measured from −0.6 (with respect to the OCP previously measured) to about 1.6 V, at a scanning rate of 0.166 $mV \cdot s^{-1}$. Current density versus potential variations was recorded, and the Tafel slopes were determined from the Evans diagrams.

Five samples (n = 5) of each manufacturing process (n = 3) were immersed in an individual glass-container with artificial saliva. All glass-containers were hermetically closed to prevent both contamination and/or evaporation of the testing solution during the incubation treatment. All containers were previously acid washed using HNO_3 2% solution and rinsed with deionized MILLI-Q water in order to prevent any contamination.

The exposed surface of the samples remained constant at approximately 125 mm^2 and the volume of the fluid was also kept constant at 50 mL, the latter was based on an extraction medium area/volume ratio of 3 cm^2/mL, according to the requirements detailed in the ISO 10993-5 Standard [40]. All the volume of the solution was extracted at different times in order to analyze the metallic ions released. Afterwards, the extracted medium was removed, filtered by passing through 0.22 µm membrane filters before diluting in HNO_3 2% solution (Suprapur, Merck, Darmstadt, Germany).

Ion-release quantification was carried out by inductively coupled plasma-mass spectrometry (ICP-MS) by using Perkin Elmer Optima 320RL equipment (Waltham, MA, USA). These measurements were carried out with samples taken at 1, 5, 24, 48, 120, 360, 700, 1000, and 1900 h. Multi-element

calibration standards were prepared by serial dilution containing Co and Cr ions at different concentrations using elemental stock solutions to prepare calibration standards. Each solution extract was analyzed in triplicate and the concentrations were determined using linear regression. An ion-release test was conducted using a Memmert Incubator Oven model BE500 (MEMMERT Gmbh, Schwabach, Germany).

3. Results and Discussion

Free corrosion potential (E_{OCP}) is determined when a steady state is reached by a corrosion system, in which both anodic and cathodic reaction rates are properly balanced with no net current flow to or from the electrode. E_{OCP} value is often used to give a qualitative indication of the corrosion regime in which a material resides, that can be categorized as active or passive as a function of their sign. In Figure 2, a measurement of E_{OCP} was used to assess how the manufacturing process affects the passivity of the alloy with time. Likewise, the Evans diagram shows the relationship of current and potential for the oxidation and the reduction reaction. These are usually plotted as potential versus the current density (*E*-*i*) curves, as can be observed in Figure 3.

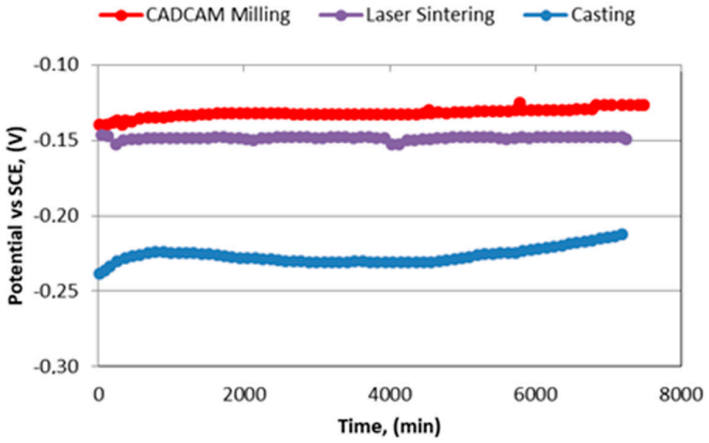

Figure 2. Corrosion potential versus time for different samples studied.

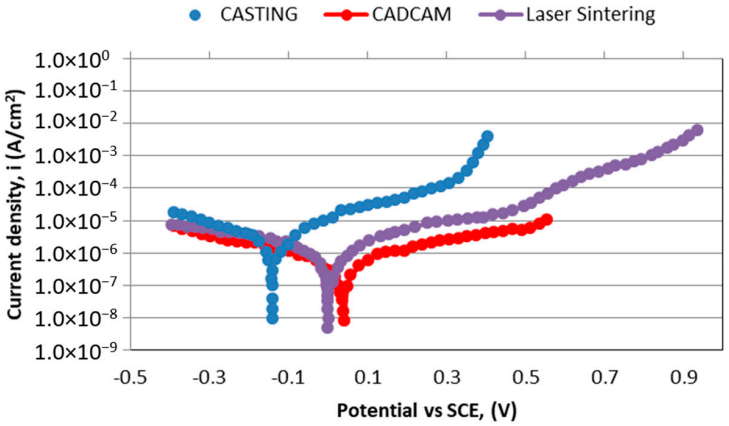

Figure 3. Polarization curves. Evans Diagrams for the samples studied.

All specimens evaluated were polarized sequentially with a total of five trials (n = 5) for each sample, which were properly polished between trials. The mean values of corrosion parameters such as critical current density (i_{corr}), corrosion potential (E_{corr}), and passive current density (i_p) were determined, as can be observed in Table 3. The results were consistent for all samples between different polarization tests for the different magnitudes. These magnitudes are defined below.

- Free corrosion potential (E_{OCP}), potential of an electrode measured with respect to a reference electrode or another electrode when no current flows to or from the material.
- Corrosion Potential (E_{corr}), potential calculated at the intersection where the total oxidation rate is equal to the total reduction rate.
- Corrosion current density (i_{CORR}), current divided by the surface of the electrode. It is the size of the anodic component of the current which flows at the corrosion potential E_{corr}. Since by definition the resulting current is equal to zero at that potential, the cathodic component is of equal size, but of opposite sign.

Table 3. Corrosion parameters analyzed.

CoCr alloy	i_{corr} (μA/cm^2)	i_p (μA/cm^2)	E_{corr} (V)
Casting	0.009	0.65	−0.18
Laser sintering	0.008	0.51	−0.01
CAD-CAM milling	0.005	0.90	+0.02

Corrosion potential is a mixed potential (also an open-circuit potential) at which the rate of anodic dissolution of the electrode equals the rate of cathodic reactions, and there is no net current flowing in or out of the electrode. Corrosion current is the dissolution current at the corrosion potential. The value of the corrosion potential indicates the state of a corroding metal while that of the corrosion current reflects the instantaneous corrosion rate at the time of measurement.

As can be observed from Figure 2, both original and CAD-CAM milled samples showed a similar natural potential around −0.13 V followed by laser sintered samples −0.15 V, while the lowest natural potential around −0.23 V corresponded to the casted samples. The original and CAD-CAM milled samples showed better natural oxidation potential (higher corrosion resistance) than the laser sintered and casted ones, which could be linked to their better chemical homogeneity. Metals higher up in the electro-chemical series (corrosion potential) displace metals lower in the series—which means that when connecting two metals with different potentials, the metal with the lowest potential corrodes [41].

As can be hinted from the graph presented in Figure 2, the analysis of the data revealed an almost constant maintenance of potential over immersion time in all samples. This signal (potential) stability would be directly connected to the proper formation of a stable Cr-oxide passive film. The stability of this inert film is due to the very small differences in volume between the Cr and its oxide. This produces an important mechanical stability of the film inhibiting the formation of both cracks and breaks. This favors the passivity of the CoCr alloys.

The corrosion potential results showed the best corrosion resistance for the CAD-CAM manufactured samples, as can be observed in the representative potentiodynamic curves presented in Figure 3. The raw material used in the CAD-CAM milling manufacturing process, commonly known as "preforms", are usually supplied in a solid block form of CoCr alloy. Such preforms are supplied with an excellent chemical and microstructural homogeneity, as a result of a proper annealing thermal pretreatment. In addition, annealing thermal pretreatment avoided the presence of residual stresses in the starting raw material, thereby helping to improve the corrosion resistance of the manufactured components.

The CAD-CAM milled samples presented a light decrease in the corrosion potential due to the residual stress induced by the machining process on the surface [7–11,39], which can enhance surface chemical reactivity during corrosion testing. As is well known, machining of metals induces residual stresses in manufactured materials which can affect their in-service behavior, as it has been reported by several authors [41,42]. This decrease in corrosion potential could be recovered with a heat treatment at 400 °C for 30 min in order to eliminate the stresses [3,4,43–45].

The laser sintered and casted samples presented low corrosion potential due to their inner heterogeneity. The melting processes totally or partially resulted in the growth of precipitates rich in

Cr, W, and Nb [43]. As a result, the matrix was enriched in Cobalt [39]. This produces an increase in current density and consequently an increase in the corrosion rate, as can be observed in Table 2.

Figure 4 shows different microstructures obtained by the three manufacturing processes used. Figure 4a corresponds to the CAD-CAM milled samples, in which equiaxial grains with twins inside can be observed. This microstructure is typical of the annealed condition without residual stress which favors the corrosion resistance [41,42]. The SEM-micrographs presented in Figure 4b correspond to the laser sintered samples, in which grains without twins may be indicative of the lack of residual stress in samples obtained by this manufacturing method. In general, the absence of twins in the same material is due to the application of stress which produces changes in the sequence of the atomic planes pilling up [44–46]. It should be noted that, after additive manufacturing steps, laser sintered samples were subsequently subjected to a stress-relieving thermal treatment. At a higher magnification of this microstructure (Figure 5), rich in Cr, W, and Nb precipitates were revealed. This chemical heterogeneity is more prone to corrosion. The casted samples showed the typical dendritic microstructure produced during the solidification process, as can be seen in Figure 4c. The microstructure of the casted samples showed the presence of a large amount of white precipitates rich in Cr, W, and Nb, which has been observed both at grain boundaries and inside grains. Microstructural analysis also reflected a coarse crystalline grain size in the casted samples, whose grains are represented in a greyscale as a function of their crystallographic orientation.

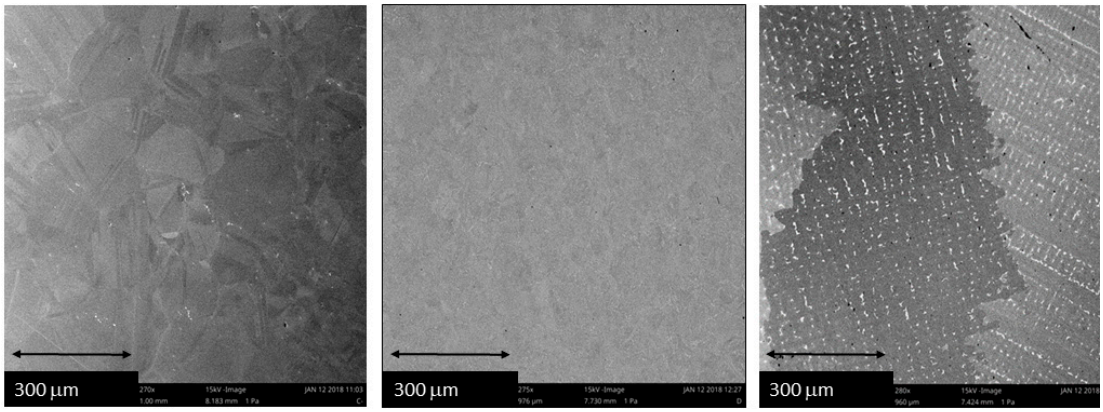

(**a**) (**b**) (**c**)

Figure 4. SEM micrographs of different microstructures obtained as a function of the manufacturing method used. (**a**) Computer-aided design and manufacturing (CAD-CAM) milling, (**b**) laser sintering, and (**c**) casting.

The higher magnification SEM micrograph of laser sintered tested samples revealed signs of localized corrosion mechanisms, as can be seen in Figure 6. Specifically, further analysis at higher magnification showed the presence of both pitting and micro galvanic corrosion mechanisms around white Cr, W, and Nb precipitates.

Ion-release results of Co and Cr ions can be observed in Figures 7 and 8, respectively. Firstly, it should be emphasized, that Co ion release rates did not reach concentrations of about 1000 ppb after 1900 h of immersion time (Figure 7). The presence of a surface passivating (inert coating) film of Cr-oxide could explain the aforementioned reduction in the ion-release rates, as such film could reduce the metallic ion diffusion to the external environment acting as a barrier layer to ion-release.

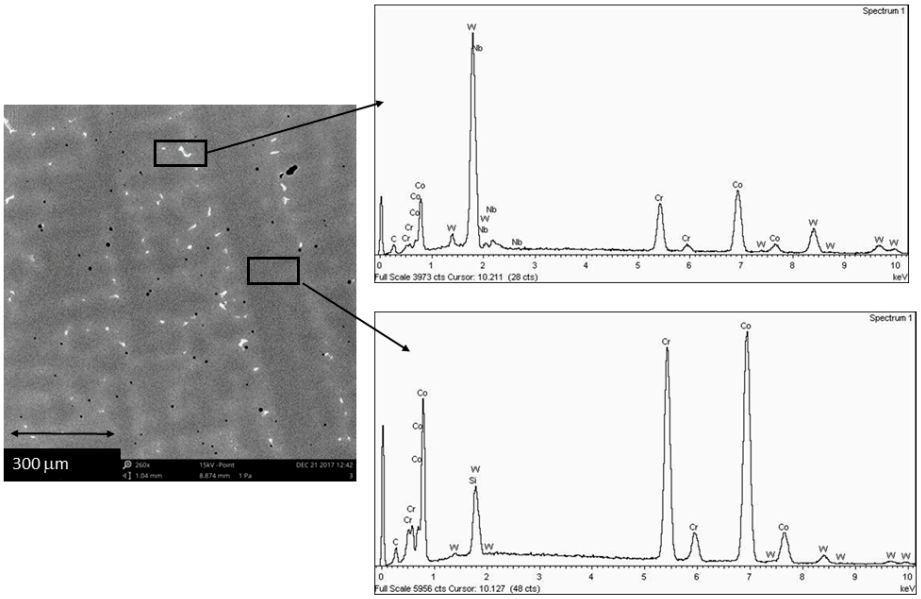

Figure 5. SEM micrograph of laser sintered sample with details of EDS-microanalysis of both the matrix and precipitates.

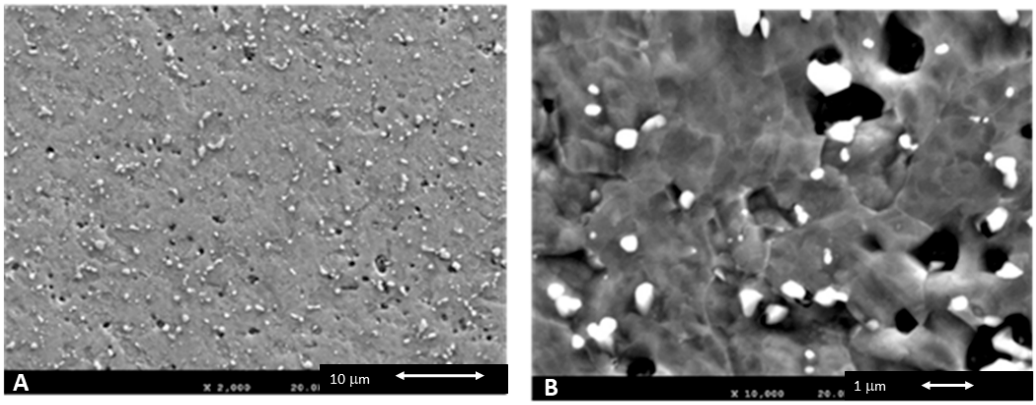

Figure 6. SEM micrographs of laser sintered corroded samples. (**A**) Generalized surface micropitting and (**B**) micro-galvanic corrosion around white Cr, W, and Nb-rich precipitates.

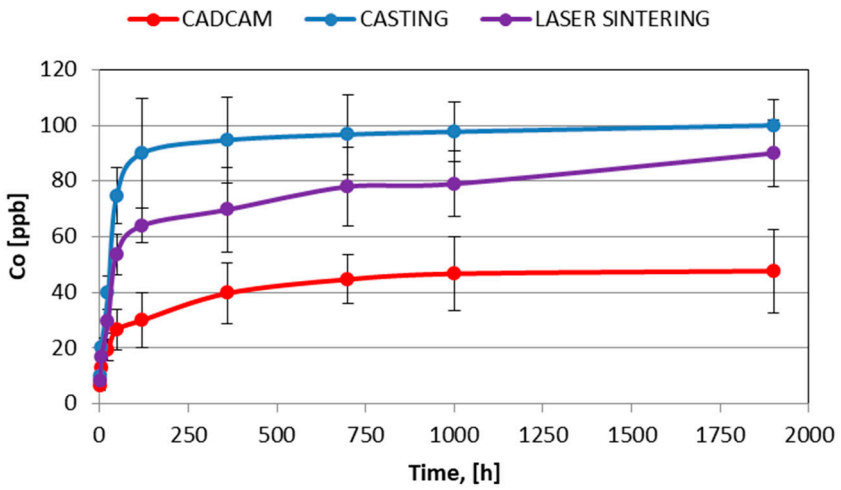

Figure 7. Co-release for different test times and types of manufacturing methods.

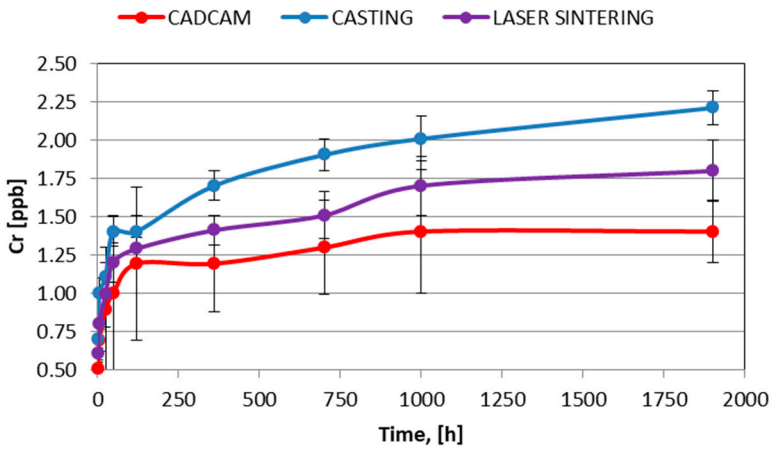

Figure 8. Cr-release for different test times and types of manufacturing methods.

Cr ion release was lower than Co due to the stabilization of this element as Cr-oxide decreasing their release to the artificial saliva. It is well known that the natural surface oxide films formed on CoCr dental alloys protect the alloys from corrosion, acting as passive barrier films [47]. These oxide films are dense as well as homogeneously distributed over the surface, which are primarily composed of Cr_2O_3. However, stability and homogeneity of these films depends on the microstructure produced by manufacturing methods [48]. Excessive volume growth of the passive oxide-film may result in cracking and partial detachment, entailing a reduction in passivation capacity. The oxide is transparent, regenerative, and is reformed spontaneously [4,8]. As can be observed from the results presented in Figure 8, Cr release rates detected were very low, near the limit of sensitivity of the equipment. The results after 1900 h were close to 2 ppb.

The typical ion release curve presented two main stages and/or regions. The initial region was characterized by a linearly constant increase in ion released to the artificial saliva, reaching a steady state for both ions after a certain time of immersion at the end of the first stage (Figure 5). In Co ion release, this change of stage was produced around 200 h of immersion. Despite the steady increase in Cr released to the liquid medium over time, Cr-ion concentration measured values were very low. Furthermore, Cr-ion release measured rates were substantially lower than those values obtained by Co-ion release. The low Cr-release rates showed in artificial saliva are an excellent observation because this ion is dangerous for the health [2,3,5,8,12]. The release rates of Chromium do not affect the human health, according to different bibliographic sources [44–49].

On the other hand, Co and Cr released ions varied depending on the manufacturing method. The casted samples showed the highest ion release rates, followed by the laser sintered and CAD-CAM milled samples, regardless of the ion analyzed. This was due to the lack of homogeneity of both the casted and laser sintered CoCr samples, the chemical heterogeneity favors the degradation and solubility of the ions. These results confirmed the findings from previous corrosion testing, suggesting that the homogeneity of CAD-CAM milled samples, without defects such as pores, volume contractions, or coring, is the optimal manufacturing method in terms of chemical stability of the dental restorations.

All samples showed total amounts of both released ions Co and Cr far below the ISO requirements [42,49–54]. In this respect, it is important to confirm that ion release and corrosion resistance are different aspects. Some researchers have suggested that low ion release rates were indicative of a good corrosion resistance. However, this affirmation cannot be generalized, given the existence of [55] metals with good corrosion resistance and high ion release rates. Corrosion is a chemical reaction whose products can be toxic, whereas ion release is a dissolution in the physiological medium. This aspect must be taken into account in order to avoid false conclusions.

4. Conclusions

Dental restorations manufactured by traditional casting methods presented lower corrosion resistance and higher Co and Cr ion release rates. The best results in terms of both corrosion and ion release behaviors corresponded to dental restorations manufactured by the CAD-CAM milling method. This is directly related to the presence of internal flaws inside the manufactured components. In this regard, both the casted and laser sintered samples have reflected the presence of defects such as pores, internal shrinkage, as well as micro segregations in the form of precipitates, among the highlights. These kinds of defects promote the appearance of micro-galvanic corrosion mechanisms, acting as corrosion accelerators. The CAD-CAM milled samples present the better results obtained in terms of ions released. In this regard, Co ion release concentration increased to 100 ppb after 1900 h of immersion, while Cr ion increased to only 2 ppb after 1900 h. This is due to the passive film of chromium oxide which is formed on the metallic surface. This oxide is very stable and avoids its release to the physiological environment.

Author Contributions: Conceptualization, F.J.G., M.H.-C., R.P.; methodology, F.J.G., M.H.-C., L.G.-T.; formal analysis, M.P., L.G.-T., M.H.-C., R.P.; investigation, R.P., M.P., F.J.G.; writing—original draft preparation, F.J.G., M.P., L.G.-T.; writing—review and editing, F.J.G., M.P., M.H.-C., R.P.; visualization, M.H.-C., L.G.-T., R.P.; supervision, F.J.G., M.H.-C., L.G.-T., M.P., R.P. All authors have read and agreed to the published version of the manuscript.

Funding: The work was supported by the Spanish government and the Ministry of Science and Innovation of Spain by the research project number RTI2018-098075-B-C21 and RTI2018-098075-B-C22, cofounded by the EU through the European Regional Development Funds (MINECO-FEDER, EU). Authors also acknowledge Generalitat de Catalunya for its funding through the 2017SGR-1165 project.

Acknowledgments: Firstly, the authors are grateful to ARCHIMEDES for its support in the research. This is an example of a company which was involved in the research.

Conflicts of Interest: The authors declare no conflict of interest.

References

1. Branemark, P.; Adell, R.; Albrektsson, T. Osseointegrated titanium implants in the rehabilitation of the edentulous patient. *Adv. Biomater.* **1982**, *4*, 133–141.
2. Ericsson, I.; Lekholm, U.; Branemark, P.; Lindhe, J.; Glantz, P.O.; Nyman, S. A clinical evaluation of fixed bridge restorations supported by the combination of teeth and osseointegrated titanium implants. *J. Clin. Periodontol.* **1986**, *13*, 307–312. [CrossRef]
3. Reclaru, L.; Meyer, J.M. Study of corrosion between a titanium implant and dental alloys. *J. Dent.* **1994**, *22*, 159–168. [CrossRef]
4. Geis-Gerstorfer, J. In vitro corrosion measurements of dental alloys. *J. Dent.* **1994**, *22*, 247–251. [CrossRef]
5. Denizoğlu, S.; YeşLilDuymuş, Z.; Akyalçin, S. Evaluation of Ion Release from Two Base-Metal Alloys at Various pH Levels. *J. Int. Med. Res.* **2004**, *1*. [CrossRef]
6. Benatti, O.F.M.; Miranda, W.G.; Muench, A. In vitro and in vivo corrosion evaluation of nickel-chromium and copper-aluminum-based alloys. *J. Prosthet. Dent.* **2000**, *84*, 360–363. [CrossRef]
7. Wataha, J.C.; Lockwood, P.E.; Khajotia, S.S. Effect of pH on element release from dental casting alloys. *J. Prosthet. Dent.* **1998**, *80*, 691–698. [CrossRef]
8. Gil, F.J.; Rodríguez, D.; Planell, J.A.; Cortada, M.; Giner, L.; Costa, S. Galvanic corrosion behaviour of Titanium implants coupled to dental alloys. *J. Mat. Sci. Mat. Med.* **2000**, *11*, 287–293.
9. Branemark, P.; Hansson, I.; Adell, R.; Lindstrom, U.; Hallen, J.; Ohman, O. Osseointegrated implants in the treatment of the edentulous jaw. Experience from a 10-year period. Scand. *J. Plast. Reconstr. Surg. Suppl.* **1977**, *16*, 1–132.
10. Adell, R.; Lekholm, U.; Rocker, U.; Branemark, P. A 15-year study of osseointegrated implants in the treatment of the treatment of the edentulous jaw. *Int. J. Oral Surg.* **1981**, *6*, 387–416. [CrossRef]
11. Sarkar, N.K.; Fuys, R.A.; Stanford, J.W. Applications of electrochemical techniques to characterize the corrosion of dental alloys. In *Corrosion and Degradation of Implant Materials*; Syrett, B.C., Acharya, A., Eds.; ASTM: Philadelphia, PA, USA, 1979; pp. 277–294.

12. Tuna, S.H.; Pekmez, N.O.; Kürkçüoğlu, I. Corrosion resistance assessment of Co-Cr alloy frameworks fabricated by CAD/CAM milling, laser sintering, and casting methods. *J. Prosthet. Dent.* **2015**, *114*, 725–734. [CrossRef]
13. Miyazaki, T.; Hotta, Y.; Kunii, J.; Kuriyama, S.; Tamaki, Y. A review of dental CAD/CAM: Current status and future perspectives from 20 years of experience. *Dent. Mater. J.* **2009**, *28*, 44–56. [CrossRef]
14. Lin, W.S.; Harris, B.T.; Zandinejad, A.; Morton, D. Use of digital data acquisition and CAD/CAM technology for the fabrication of a fixed complete dental prosthesis on dental implants. *J. Prosthet. Dent.* **2014**, *111*, 1–5. [CrossRef]
15. Kim, K.B.; Kim, W.C.; Kim, H.Y.; Kim, J.H. An evaluation of marginal fit of three-unit fixed dental prostheses fabricated by direct metal laser sintering system. *Dent. Mater.* **2013**, *29*, 91–96. [CrossRef]
16. Akova, T.; Ucar, Y.; Tukay, A.; Balkaya, M.C.; Brantley, W.A. Comparison of the bond strength of laser-sintered and cast base metal dental alloys to porcelain. *Dent. Mater.* **2008**, *24*, 1400–1404. [CrossRef]
17. Ucar, Y.; Akova, T.; Akyil, M.S.; Brantley, W.A. Internal fit evaluation of crowns prepared using a new dental crown fabrication technique: Laser-sintered Co-Cr crowns. *J. Prosthet. Dent.* **2009**, *102*, 253–259. [CrossRef]
18. Atzeni, E.; Salmi, A. Evaluation of additive manufacturing (AM) techniques for the production of metal–ceramic dental restorations. *J. Manuf. Process.* **2015**, *20*, 40–45. [CrossRef]
19. Chen, J.; Zhang, Z.; Chen, X.; Zhang, C.; Zhang, G.; Xu, Z. Design and manufacture of customized dental implants by using reverse engineering and selective laser melting technology. *J. Prosthet. Dent.* **2014**, *112*, 1088–1095. [CrossRef]
20. Hongfu, Z.; Qin, F. 3D reconstruction and SLM survey for dental implants. *J. Mech. Med. Biol.* **2017**, *17*, 1750084.
21. Beuer, F.; Aggstaller, H.; Ritcher, J.; Edelhoff, D.; Gernet, W. Influence of preparation angle on marginal and internal fit of CAD/CAM fabricated zirconia crowns copings. *Quintessence Int.* **2009**, *40*, 419–424.
22. Borba, M.; Cesar, P.F.; Griggs, J.A.; Della Bona, A. Adaptation of all-ceramic fixed partial dentures. *Dent. Mater.* **2011**, *27*, 1119–1126. [CrossRef]
23. Coli, P.; Karlsson, S. Fit of a new pressure sintered zirconium dioxide coping. *Int. J. Prosthod.* **2004**, *17*, 59–64.
24. Colpani, J.T.; Borba, M.; Della Bona, A. Evaluation of marginal and internal fit of ceramic crown copings. *Dent. Mater.* **2013**, *29*, 174–180. [CrossRef]
25. Naert, I.; van Der Donck, A.; Beckers, L. Precision of fit and clinical evaluation of all-ceramic full restorations followed between 0.5 and 5 years. *J. Oral Rehabil.* **2005**, *32*, 51–57. [CrossRef]
26. Rödiger, M.; Schneider, L.; Rinke, S. Influence of Material Selection on the Marginal Accuracy of CAD/CAM-Fabricated Metal- and All-Ceramic Single Crown Copings. *Biomed. Res. Int.* **2018**, *2018*, 2143906. [CrossRef]
27. Sannino, G.; Gloria, F.; Schiavetti, R.; Ottria, L.; Barlattani, A. Dental wings cad/cam system precision: An internal and marginal fit sperimental analisys. *Oral Implantol.* **2009**, *2*, 11–20.
28. Sailer, I.; Makarov, N.A.; Thoma, D.S.; Zwahlen, M.; Pjetursson, B.E. All-ceramic or metal-ceramic tooth-supported fixed dental prostheses (FDPs)? A systematic review of the survival and complication rates. Part I: Single crowns (SCs). *Dent. Mater.* **2015**, *31*, 603–623. [CrossRef]
29. Nedelcu, R.; Olsson, P.; Nyström, I.; Thor, A. Finish line distinctness and accuracy in 7 intraoral scanners versus conventional impression: An In Vitro descriptive comparison. *BMC Oral Health* **2018**, *18*, 27. [CrossRef]
30. Aldegheishem, A.; Ioannidis, G.; Att, W.; Petridis, H. Success and survival of various types of all-ceramic single crowns: A critical review and analysis of studies with a mean follow-up of 5 years or longer. *Int. J. Prosthodont.* **2017**, *30*, 168–181. [CrossRef]
31. Rinke, S.; Fornefett, D.; Gersdor, N.; Lange, K.; Roediger, M. Multifactorial analysis of the impact of different manufacturing processes on the marginal t of zirconia copings. *Dent. Mater.* **2012**, *31*, 601–609. [CrossRef]
32. Brugirard, J. *Etude du Comportament Électrochimique des Métaux et Alliages Dentaires*; J Prelat: Paris, France, 1970; pp. 62–68.
33. Correa, C.B.; Pires, J.R.; Fernandes-Filho, R.B.; Sartori, R.; Vaz, L.G. Fatigue and fluoride corrosion on *Streptococcus mutans* adherence to titanium-based implant/component surfaces. *J. Prosthodont.* **2009**, *18*, 382–387. [CrossRef]
34. ASTM-E3-11. *Standard Guide for Preparation of Metallographic Specimens*; ASTM International: West Conshohocken, PA, USA, 2017.

35. Baboian, R. Electrochemical techniques for predicting galvanic corrosion. In *Galvanic and Pitting Corrosion-Field and Laboratory Studies*; Baboian, R., France, W., Rowel, L., Ryniewicz, J., Eds.; ASTM: Philadelphia, PA, USA, 1976; pp. 5–19.
36. Mansfeld, F.; Kenkel, J.V. Laboratory studies of galvanic corrosion of aluminium alloys. In *Galvanic and Pitting Corrosion-Field and Laboratory Studies*; Baboian, R., France, W., Roew, L., Rynewicz, J., Eds.; ASTM: Philadelphia, PA, USA, 1976; pp. 20–47.
37. Mansfeld, F. The Polarization Resistance Technique for Measuring Corrosion Currents. In *Advances in Corrosion Science and Technology*; Fontana, M.G., Staehle, R.W., Eds.; Springer: Boston, MA, USA, 1976; pp. 89–92.
38. Canay, S.; Öktemer, M. In Vitro corrosion behaviour of 13 prosthodontic alloys. *Dent. Res.* **1992**, *23*, 279–287.
39. American Society for Testing and Materials. *Standard Reference Test Method for Making Potentiostatic and Potentiodynamic Anodic Polarization Measurements*; Technical Report No. ASTM G5-14e1; ASTM International: West Conshohocken, PA, USA, 2014.
40. IOS. *ISO 10993-5:2009. Biological Evaluation of Medical Devices—Part 5: Tests for In Vitro Cytotoxicity*; International Organization for Standardization: Geneve, Switzerland, 2009.
41. Al Jabbari, Y.S. Physico-mechanical properties and prosthodontic applications of Co-Cr dental alloys: A review of the literature. *J. Adv. Prosthodont.* **2014**, *6*, 138–145. [CrossRef]
42. Al Jabbari, Y.S.; Barmpagadaki, X.; Psarris, I.; Zinelis, S. Microstructural, mechanical, ionic realese and tarnish resistance characterization of porcelain fused to metal Co-Cr alloys manufactured via casting and three different CAD/CAM techniques. *J. Prosthod. Res.* **2019**, *63*, 150–156. [CrossRef]
43. Gil, F.J.; Sánchez, L.A.; Espias, A.; Planell, J.A. In vitro corrosion behaviour and metallic ion release of different prosthodontic alloys. *Int. Dent. J.* **1999**, *49*, 347–351. [CrossRef]
44. Aparicio, C.; Rodriguez, R.; Manero, J.M.; Andrés, A.; Arandés, J.; Planell, J.A. *Aleaciones Ligeras*; Gil, F.J., Ed.; Ediciones UPC: Barcelona, Spain, 2001; pp. 480–487.
45. Porter, D.A.; Easterling, K.E.; Sheriff, M. *Phase Transformation in Metals and Alloys*, 3rd ed.; CRC Press: Boca Raton, FL, USA, 2013.
46. Velasco, E.; Monsalve-Guil, L.; Jimenez, A.; Ortiz, I.; Moreno-Muñoz, J.; Nuñez-Marquez, E.; Pegueroles, M.; Perez, R.; Gil, F.J. Importance of the Roughness and Residual Stresses of Dental Implants on Fatigue and Osseointegration Behavior. In Vivo Study in Rabbits. *J. Oral Inv.* **2016**, *42*, 469–476. [CrossRef]
47. Al-Hity, R.R.; Kappert, H.F.; Viennot, S.; Dalard, F.; Grosgogeat, B. Corrosion resistance measurements of dental alloys, are they correlated? *Dent Mater.* **2007**, *23*, 679–687. [CrossRef]
48. Galo, R.; Rocha, L.A.; Faria, A.C.; Silveira, R.R.; Ribeiro, R.F.; de Mattos, M.D.G. Influence of the casting processing route on the corrosion behavior of dental alloys. *Mater. Sci. Eng.* **2014**, *45*, 519–523. [CrossRef]
49. Molina, C.; Nogués, L.l.; Martinez-Gomis, J.; Peraire, M.; Salsench, J.; Sevilla, P.; Gil, F.J. Dental casting alloys behaviour during power toothbrushing with toothpastes with various abrasivities. Part II: Corrosion and ion release. *J. Mater. Sci. Mater. Med.* **2008**, *19*, 3015–3019. [CrossRef]
50. Vallet-Regí, M.; Izquierdo-Barba, I.; Gil, F.J. Localized corrosion of 316L stainless steel with SiO_2-CaO films obtained by means of sol-gel treatment. *J. Biomed. Mater. Res.* **2003**, *67*, 674–678. [CrossRef]
51. Kim, H.R.; Jang, S.H.; Kim, Y.K.; Son, J.S.; Min, B.K. Microstructures and mechanical properties of CoCr dental alloys fabricated by three CAD/CAM based processing techniques. *Materials* **2016**, *9*, 596. [CrossRef] [PubMed]
52. Aparicio, C.; Gil, F.J.; Fonseca, C.; Barbosa, M.; Planell, J.A. The effect of shot blasting and heat treatment on the fatigue behavior of titanium for dental implant applications. *Dent. Mater.* **2007**, *23*, 486–491.
53. Subbu, R.; Sagoo, R.; Goswami, V.; Goswami, K.; Langman, G.; Bhatt, K.; Roy-Choudhury, S. Metallosis in metal-on-metal hip resurfacing: An unusual presentation. *Eur. J. Radiol. Extra* **2011**, *78*, 101–104. [CrossRef]
54. Hosoki, M.; Bando, E.; Asaoka, K.; Takeuchi, H.; Nishigawa, K. Assessment of allergic hypersensivity to dental materials. *Biomed. Mater. Eng.* **2009**, *19*, 53–61.
55. Mombelli, A.; Hashim, D.; Cionca, N. What is the impact of titanium particles and bioocorrosion on implant survival and complications? A critical review. *Clin. Oral Impl. Res.* **2018**, *29*, 37–53. [CrossRef]